Wiley
Advances in Materials Science and Engineering
Volume 2025, Article ID 8059229, 16 pages
https://doi.org/10.1155/amse/8059229

WILEY

Research Article

Triboelectrochemical Performance of Electron Beam–Melted Ti-6Al-4V-ELI for Biomedical Applications

E. F. Pieretti,[1,2,3] **L. C. E. Silva**,[1] **M. S. Ribeiro**,[1] **W. de Rossi**,[1] **R. A. Antunes**,[2] **M. C. L. Oliveira**,[2] **D. Piaggio**,[3] **F. P. A. Cruz**,[4] **J. O. da Paz**,[4] **and M. D. M. das Neves**[1]

[1]*Nuclear and Energy Research Institute, National Nuclear Energy Commission, São Paulo, Brazil*
[2]*Center for Engineering, Modeling and Applied Social Sciences, Federal University of ABC, Santo André, São Paulo, Brazil*
[3]*School of Engineering, University of Warwick, West Midlands, Coventry, UK*
[4]*Ortossintese Ltda, São Paulo, Brazil*

Correspondence should be addressed to E. F. Pieretti; eurico.pieretti@warwick.ac.uk

Received 26 February 2025; Revised 1 August 2025; Accepted 2 September 2025

Academic Editor: Mohammad Rezwan Habib

Titanium alloys have been widely used for biomaterials' production due to their high physicochemical stability, mechanical resistance, and biocompatibility. Currently, additive manufacturing (AM) techniques using electron beam melting (EBM) technology have been used to produce implantable medical and dental devices. In the present work, the effect of five different scanning speed on the tribocorrosion behavior of Ti-6Al-4V-ELI (extra low interstitials) alloy was evaluated in Ringer's saline solution, at 25°C, under a 10-N normal force in both cathodic and anodic regions to provide a basis for properly deriving the tribological constants of this EBM alloy. A tribometer coupled with a potentiostat/galvanostat, was used to rub the Ti-6Al-4V-ELI disks against alumina balls. The tribocorrosion tests were carried out for 50 min for each sample. The open circuit potential and corrosion current densities were monitored for 10 min, then concomitant with wear tests during 30 min, and finally for more 10 min, without wear. The scratched surfaces were characterized by confocal laser scanning microscopy. The results indicated that the tribocorrosion behavior is influenced by the Ti-6Al-4V-ELI surface finishing. The open circuit potential quickly dropped from −0.55 to −0.75 ($V/_{Ag/AgCl}$) for all samples during tribological application, then returned to nobler values after the application was removed, with the highest values being obtained for Disks 2 and 4. An opposite effect was observed during the chronoamperometry tests. The wear rate depends on the electrolyte, which serves as both a corrosive environment and a tribological lubricant and is closely linked to the speed variation in the EBM manufacturing process. In all cases, the disks produced with EBM scan speed Parameters 1 and 5 showed the highest wear rates.

Keywords: biomedical devices; confocal microscopy; electron beam melting; titanium alloys; tribocorrosion

1. Introduction

Biomaterials, once implanted, are subject to several types of premature failure, such as wear, fatigue, micromovements, particle detachment, and degradation, which may generate the need for new surgical interventions [1, 2]. In fact, implantable medical devices, as they are in direct contact with body fluids, are exposed to an environment rich in chloride ions that trigger the localized corrosion process [3–8].

Currently, additive manufacturing (AM) is widely used for manufacturing implant devices, either using selective laser melting (SLM) or electron beam melting (EBM) technologies. The surfaces obtained by these processes are covered with a certain amount of adhered material, which is partially melted. This is considered a disadvantage of melting-based techniques using a bed of particulate materials, which prevents the achievement of a smooth surface. The undesirable adhesion of partially molten particles to the surface of a component manufactured by SLM or EBM can

be attributed to heterogeneous heat flow, thermal diffusivity, and partial melting of particles in the boundary layer with laser beam or electron beam. In fact, a high temperature difference between powder particles and those positioned in the powder bed of molten material causes melting and adhesion to the product surface [9–12].

For implants that interface with bones, surfaces that are rough, have porous coatings, or exhibit osteoconductive and osteoinductive properties for body fluids are ideal for osseointegration. Specifically, for titanium and its alloys, rough surfaces are advantageous in promoting mechanical fixation, enhancing stress distribution at the bone-implant interface, and facilitating osseointegration [13]. Nonetheless, surfaces with too high roughness can favor the development of bacteria in regions with low blood supply and act as stress risers when the implantable device is subject to fatigue loadings [14].

Researches have demonstrated that components fabricated with titanium and its alloys using SLM and EBM methods exhibit enhanced osseointegration. However, these components require supplementary surface finishing processes to achieve optimal osseointegration performance [15, 16].

In fact, the surface finishing conditions of biomaterials directly affect various surface properties, including electrochemical and tribological responses. Rougher surfaces reduce resistance to localized corrosion [1] and wear [17]. This effect can be evaluated individually or concomitantly, through tribocorrosion, which is the combined effect of tribology and corrosion in a chemically active mechanical system. Recent studies on different alloys are available, but the impact of varying processing parameters, such as scanning speed, is not thoroughly explored.

The Ti-6Al-4V alloy has attracted much interest in developing EBM-based materials due to its mature technological applications in the biomedical field, which are a direct consequence of its well-known inherent biocompatibility, high strength-to-weight ratio, and excellent corrosion resistance [18]. Silvestri et al. [19] have shown that EBM processing parameters, such as scan speed and beam current, may influence the microstructure and surface roughness of the Ti-6Al-4V alloy due to the different amounts of energy absorbed by the alloy.

The corrosion behavior of EBM-manufactured Ti alloys has been investigated by several authors [20–23]. Abdeen and Palmer [24] studied the corrosion resistance of an EBM-process Ti-6Al-4V alloy in 3.5 wt.% NaCl solution at temperatures ranging from 20°C to 85°C, comparing the results with a conventionally manufactured wrought counterpart. Both the EBM and wrought Ti-6Al-4V alloys exhibited a wide passive range and high corrosion resistance even at the highest testing temperature. Dehnavi et al. [25] investigated the corrosion resistance of EBM Ti-6Al-4V in 3.5 wt.% NaCl solution at room temperature. The electrochemical behavior was also compared with a conventional wrought Ti-6Al-4V counterpart. The corrosion resistance of the EBM alloy was found to be slightly lower than that of the wrought material. This behavior was associated with microstructural aspects. The EBM samples showed a heterogeneous distribution of alloying elements segregated in the grains of the β-phase, especially Fe. Moreover, they exhibited a Widmanstätten-type microstructure that was more susceptible to corrosion than the equiaxed grains of the wrought alloy, as reported in the literature [26, 27].

Also, the wear behavior of EBM alloys has been studied in the literature [28, 29]. The worst abrasive wear of EBM Ti-6Al-4V alloy concerning a conventional wrought Ti-6Al-4V alloy was observed by Herrera et al. [28]. The lamellar ($\alpha + \beta$) microstructure of the EBM sample (compared to the homogeneous globular microstructure of the wrought sample) and its relatively high porosity level (6.8 times higher than the wrought sample) were responsible for the increased propensity to wear. Sharma et al. [29] showed that the wear loss of EBM Ti-6Al-4V samples was dependent on the microstructure and could be controlled by heat treatments that were able to modify coarser β-phase grains and produce a refined hard martensitic structure.

As regards tribocorrosion tests, they have been conducted for conventional Ti alloys [30, 31]. For example, Hacisalihoglu et al. [32] studied the tribocorrosion behavior of several titanium alloys in Kokubo's solution by combining linear reciprocating wear tests and electrochemical tests. The wear tests were conducted against alumina balls at a constant normal load of 2 N. They showed the influence of alloy microstructure on the wear properties.

In the same regard, as AM technologies advance and new materials are developed, the need for evaluating the tribocorrosion behavior of EBM-manufactured alloys increases. Hence, it is possible to find recent information in the literature regarding different alloys, although the effect of varying processing parameters, such as scanning speed, has not been extensively investigated. For instance, Shittu et al. [33] evaluated the concomitant effect of wear and corrosion on the tribocorrosion response of a CoCrFeMnNi high entropy alloy plates manufactured by laser-engineered net shaping (LENS) AM process. The AM-processed alloy exhibited a lower wear rate than its conventional counterpart due to the refined microstructure obtained by the laser-based process. Buciumeanu et al. [34] used the same AM process to produce NiTi and Ti-6Al-4V samples. The tribocorrosion behavior of the AM-processed samples was assessed using reciprocating ball-on-disc wear tests, and the electrolyte was a phosphate-buffered solution (PBS). Abrasion of the metallic surface played a major role in the wear mechanism during the tribocorrosion tests. Toptan et al. [35] and Huang et al. [36] have also studied the tribocorrosion behavior of Ti-6Al-4V obtained by a laser-based AM process (SLM). The relationship between alloy microstructure, surface oxide film, and applied potential was important to understand the simultaneous action of wear and corrosion. Conversely, while the individual corrosion and wear behaviors of EBM Ti alloys have been investigated, their simultaneous action has been hardly studied.

Further investigation into the parameters of AM, such as its velocity, is necessary to enhance the efficiency of device production and reduce waste related to energy and equipment usage. This effect can be evaluated individually or mutually through tribocorrosion tests. The corrosion, wear,

and failure of metallic biomaterials are critical concerns in the long-term performance of medical implants. Understanding the interaction between these phenomena and the biological environment is essential for improving the longevity and safety of biomedical devices. Advances in biomaterials processing technology, surface modification techniques, and failure analysis tools are helping to optimize material properties, reduce failure rates, and enhance the biocompatibility of metallic biomaterials in medical applications. Although recent studies address various alloys, the effect of different processing parameters, such as scanning speed, has not been extensively explored. The aim of the present work is to fill this gap. In this respect, tribocorrosion tests of an EBM Ti-6Al-4V-ELI alloy obtained at five different scan speeds were conducted. The purpose of changing the scan speed parameter is to produce AM devices in a faster and inexpensive way. A tribometer operating in the ball-on-disk geometry was employed for the wear tests. The electrochemical tests were conducted in Ringer's solution.

2. Materials and Methods

2.1. Material and Sample Preparation. The Ti-6Al-4V-ELI (extra low interstitials) powder, purchased from AP&C Inc. Québec, Canada, was used to obtain five samples in disk format with 90 mm in diameter, and 8 mm in height, by EBM technique, at 5 different scanning speed parameters: (1) 4077, (2) 4300, (3) 4530, (4) 4757, and (5) 4983 ($mm{\cdot}s^{-1}$). The industry speed parameter commonly used is Number 3. Changes in equipment scanning speeds are limited to increments of 1%, 5%, and 10%. Increases of 1% in speed do not result in significant changes; therefore, this work aims to evaluate samples made with 5% and 10% lower and higher than the scanning speed currently used. The equipment utilized was an Arcam Q10 plus EBM 3D printer machine, with print space dimensions: $200 \times 200 \times 180$ mm, electron beam with a spot size of 100 μm generated at a voltage of 60 kV, and a beam power of 6.2 W. The layer thickness was adjusted to 50 μm, and the plate preheating was 554°C. The powder chemical composition, particle size distribution, flow rate, and apparent and tap densities are shown in Table 1. The surface characterization was conducted using a scanning electron microscope (SEM-EDX), Model TM3000 (Hitachi, Japan), and the particle image is shown in Figure 1. All the samples' surface finishes were sanded to 2400 grid SiC and cleaned in ultrasound with deionized water.

2.2. Tribocorrosion Tests. The tribocorrosion experiments were conducted in a ball-on-disk tribometer (Ducom Instrument, MicroPoD) coupled with a potentiostat/galvanostat (Iviumn n-Stat). The wear rate was calculated using the Archard's wear equation (1), which relates wear volume to normal load, sliding distance, and material hardness, assuming wear is proportional to real contact area and sliding distance. It is typically measured in mm^3/m, $\mu m^3/m$, or mm^3/Nm.

Table 1: Ti-6Al-4V-ELI (ASTM F30001) powder characteristics.

Chemical composition (wt%)		
Ti	Al	V
Bal.	6.34 ± 0.05	3.98 ± 0.02
Particle size distribution (ASTM B822)		
D10	D50	D90
51.0 ± 0.03	69.0 ± 0.04	96.2 ± 0.03
Flow rate ($s{\cdot}50\ g^{-1}$)	Apparent density ($g{\cdot}cm^{-3}$)	Tap density ($g{\cdot}cm^{-3}$)
25.0 ± 0.03	2.58 ± 0.01	2.8 ± 0.03

Note: ($n = 3$). ($p < 0.05$).

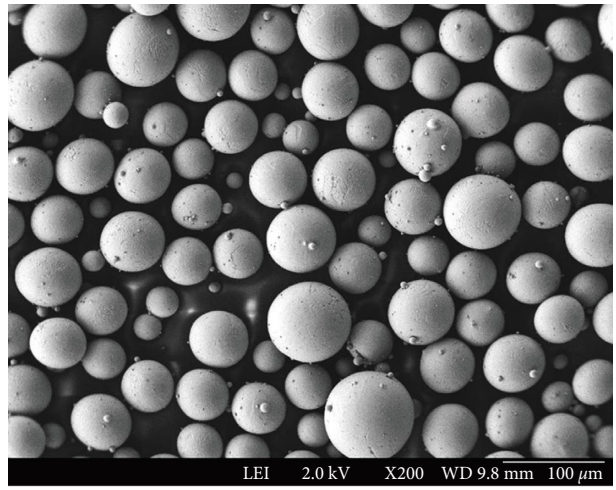

Figure 1: SEM image of Ti-6Al-4V-ELI (ASTM F30001) powder particles, illustrating the spherical character and its size distribution.

$$V = K\frac{WL}{H}, \tag{1}$$

where V is wear volume, K is wear coefficient, W is normal load, L is sliding distance, and H is hardness.

A cell with a three-electrode arrangement was used: the EBM Ti-6Al-4V ELI disk as the work electrode, a platinum wire as the counter-electrode, and an Ag/AgCl (KCl, 3 M) electrode as the reference.

The tribocorrosion tests lasted 50 min, divided into the following three stages: (i) 10 min of electrochemical monitoring, (ii) 30 min of electrochemical and tribology evaluation, and (iii) 10 min of electrochemical monitoring (without wear). Solid ceramics spheres of alumina (Al_2O_3), with a diameter of 6 mm, were used as counter-bodies. The wear tests were performed with a normal force of 10 N and at a sliding frequency of 1 Hz. The electrolyte was Ringer's solution at 25°C. Current density and/or open circuit potential (OCP) versus time were monitored throughout the test. Two distinct potentials were employed for the tests: OCP and +0.4 ($V/_{Ag/AgCl}$) (disk under anodic polarization). For the tests conducted at the OCP condition, the electrochemical potential was continuously monitored, whereas the current density was monitored for the tests conducted at +0.4 ($V/_{Ag/AgCl}$).

For comparison purposes, tribological tests were also conducted for 30 min, in order to evaluate the friction properties at the same conditions used for tribocorrosion tests (normal load of 10 N and frequency of 1 Hz, using 6-mm diameter alumina balls as counter bodies).

2.3. Surface Morphology. A LEXT OLS 4100 (Olympus, TM) confocal laser scanning microscope (CLSM) was used to measure the roughness (Ra) of the EBM Ti-6Al-4V-ELI samples. The wear tracks were also examined at least six times per sample ($n = 6$) by CLSM using the same instrument.

2.4. Statistical Analysis. Experimental data were expressed as mean ± SD. Independent *t*-test was performed to compare the values of two groups, and one-way ANOVA was carried out to perform multiple group comparisons. All statistical analyses were conducted by the software of SPSS Version 23.0, and a $p < 0.05$ was set as a significant difference.

3. Results and Discussion

When it comes to biomaterials for implantable medical or dental devices, tribological tests are important in providing an estimate of the normal and frictional forces concerning the volume of material that can be detached from the surface, migration, and accommodation of some particles. The sample number sequence presented refers to the electron beam scanning speed, as mentioned above. The aim of evaluating the tribological and corrosion behavior of these samples by changing the speed parameter is to produce implantable devices more quickly, with energy savings, lower operator costs, and less time using the equipment. In this work, the terminology tribology disk means the samples used for tribocorrosion tests, and wear tracks refers to the visible signs of surface damage that occur when Al_2O_3 spheres rub against the Ti–6Al–4V–ELI samples under load. All the tribocorrosion tests were repeated three times per sample in order to confirm the reproducibility of these results ($n = 3$).

3.1. Tribocorrosion Analyses. The monitoring data of the corrosion open-circuit potential for Ti-6Al-4V– ELI samples produced at five different EBM scan speeds are shown in Figure 2. The three aforementioned stages are evident: the open-circuit potential drastically changes its behavior during the complete 50-min test.

For each type of sample, the corrosion potential *E* ($V/_{Ag/AgCl}$) showed a similar behavior, starting at potentials around −0.2 and −0.45 ($V/_{Ag/AgCl}$) during the first periods until 600 s; from 600 to 2400 s, the potential is monitored concomitant to wear tests, and after 2400 s, only the corrosion potential is monitored again. All samples showed a quick decrease in potential to the order of −0.55 to −0.75 ($V/_{Ag/AgCl}$), which is in accordance with the literature [37, 38]. The wear tests were carried out during 1800 s and, after this time, the potential values tended to rise to the order of −0.1 to −0.4 ($V/_{Ag/AgCl}$). At the end of the test, Samples 2 and 4 presented a corrosion potential higher than their value at the starting moment. Samples 3 and 5 ended the test with corrosion potential values lower than their values at the beginning of the test. Sample 1 showed a corrosion potential at the end similar to that obtained in the first periods of immersion.

The OCP is widely employed to assess the chemical stability and corrosion processes of specimens. Fellah et al. [37] studied the variation of the OCP in Ti50-Ni50 samples produced at different milling periods, when immersed in Hank's solution. The results indicated that the OCP values increased with immersion time and subsequently stabilized. This behavior suggests the formation of a passive film on the surface of the samples, which enhances corrosion resistance by acting as a barrier against metal ion release. Similar observations were made for EBM Ti-6Al-4V-ELI samples after tribological assessment.

The tribocorrosion cycle starts with the mechanical abrasion of the passive layer and concludes with the reformation of the passive oxide layer [38].

The chronoamperometry results are shown separately for each type of tribology disk (Figure 3) due to their corrosion current density (Icorr) values, which are in the order of milliamperes and microamperes. The corrosion current values rose rapidly with the start of the tribological test and returned to lower levels at the end, after 30 min of wear, and remained at these lower values until the test was complete. Figure 3(a) shows the tribocorrosion current evaluation for Sample 1, with the mechanical abrasion starting at 600 s and ending at 2400 s.

The chronoamperometry tests were done at a fixed −0.4 ($V/_{Ag/AgCl}$) potential. The corrosion current density (Icorr) values for all samples showed a quick increase in current during the wear tests, then decreasing after this. Samples 1 and 5 showed current densities in the order of microamperes, while Samples 2, 3, and 4 showed current densities in the order of milliamperes. Sample 1 currents rose when the wear test started and reached higher values at the end of the test. In Sample 2, the current density increased faster at the wear starting time, then decreased continuously until the end, as shown in Figure 3(b). In Figure 3(c), the tribocorrosion current evaluation for Sample 3 is shown; the current density increased at 600 s, and in the middle of the wear test, it started to decrease. Figure 3(d) presents the chronoamperometry test for Sample 4; it shows a well-defined homogeneous behavior of the current, increasing at 600 s, remaining stable, and then decreasing at 2400 s until the end; a similar behavior is observed for Sample 5 in Figure 3(e). As described in the literature [39], starting the friction, the current moved to a more anodic zone and returned to the original stages once the rubbing was finished.

Analyses using potentiometry and chronoamperometry demonstrated the passive characteristics of the oxide film that naturally formed on the surfaces of this biomaterial.

The tribological evaluation associated with the corrosion OCP monitored, for all five disks, is shown in Figures 4, 5, 6, and 7.

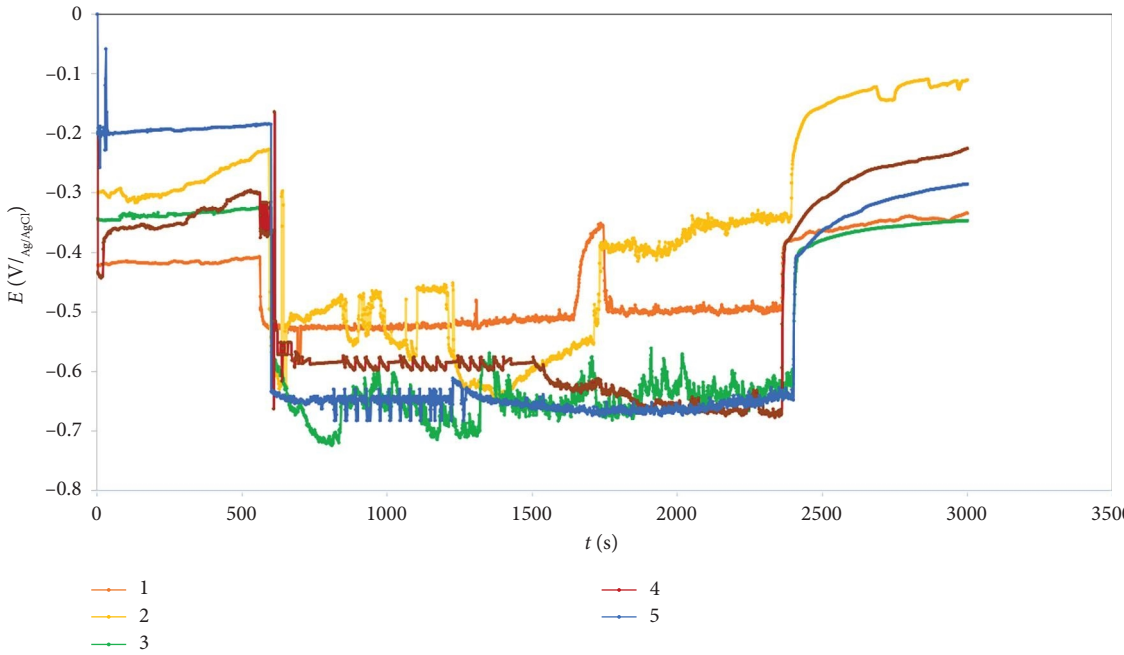

Figure 2: Tribocorrosion evaluation of the OCP monitoring in function of time for the five types of tribology disks. Total test time: 3000 s ($n = 3$).

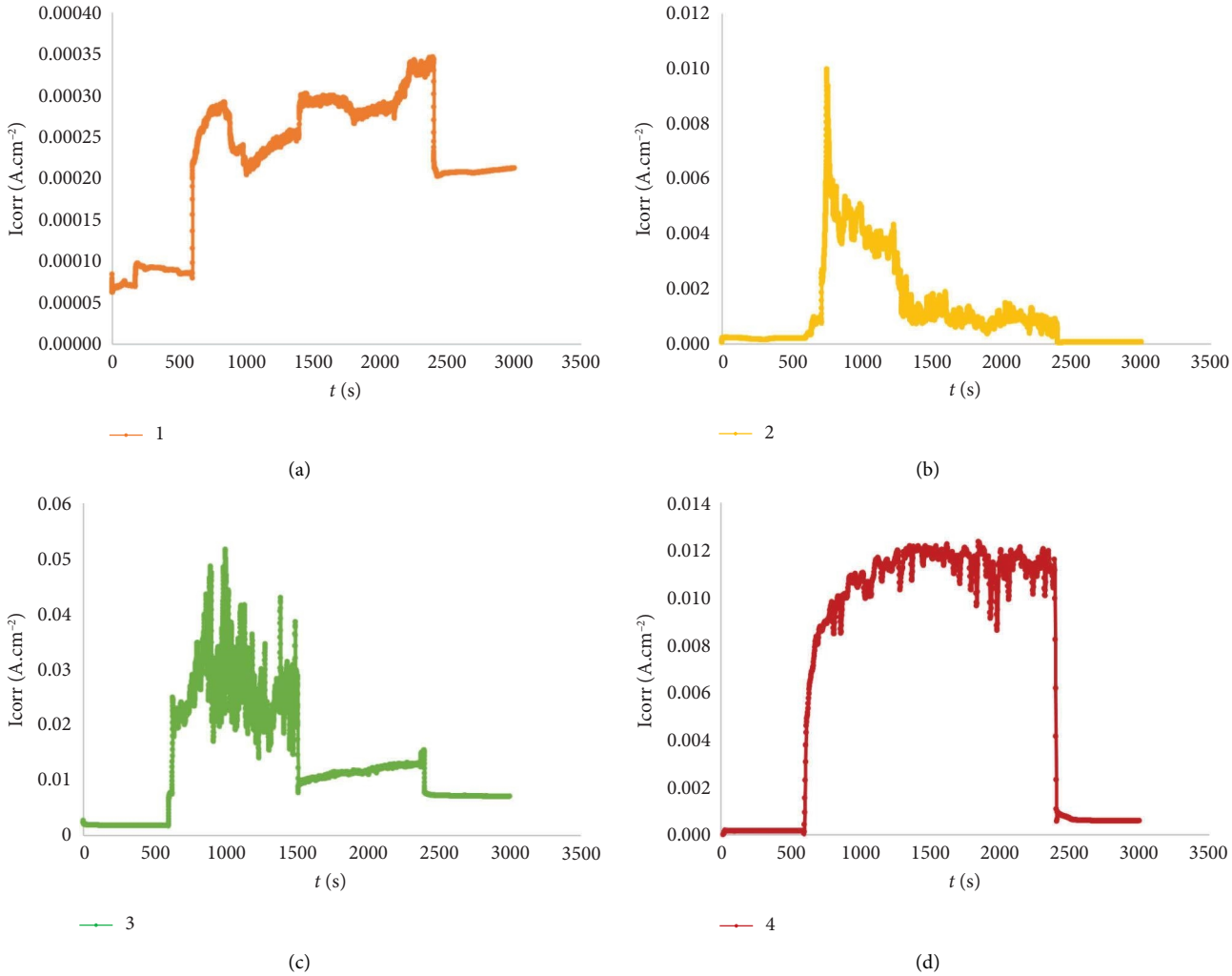

Figure 3: Continued.

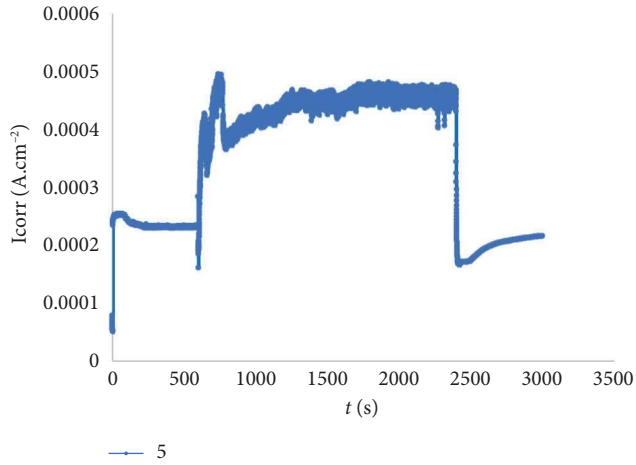

(e)

Figure 3: (a) Tribocorrosion evaluation of the corrosion current density monitoring in function of time for the tribology Disk 1. EBM scanning speed: 4077 mm·s^{-1}. Mechanical abrasion time: 1800 s. Total test time: 3000 s, ($n = 3$). (b) Tribocorrosion evaluation of the corrosion current density monitoring in function of time for the tribology Disk 2. EBM scanning speed: 4300 mm·s^{-1}. Mechanical abrasion time: 1800 s. Total test time: 3000 s ($n = 3$). (c) Tribocorrosion evaluation of the corrosion current density monitoring in function of time for the tribology Disk 3. EBM scanning speed: 4530 mm·s^{-1}. Mechanical abrasion time: 1800 s. Total test time: 3000 s ($n = 3$). (d) Tribocorrosion evaluation of the corrosion current density monitoring in function of time for the tribology Disk 4. EBM scanning speed: 4757 mm·s^{-1}. Mechanical abrasion time: 1800 s. Total test time: 3000 s ($n = 3$). (e) Tribocorrosion evaluation of the corrosion current density monitoring in function of time for the tribology Disk 5. EBM scanning speed: 4983 mm·s^{-1}. Mechanical abrasion time: 1800 s. Total test time: 3000 s ($n = 3$).

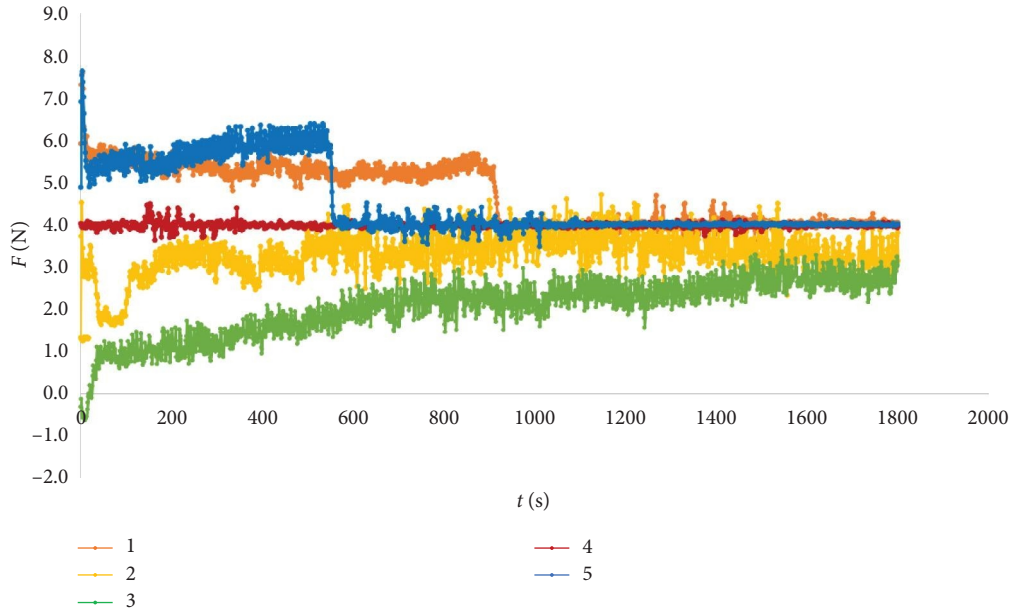

Figure 4: Frictional force variation in function of time for all types of tribology disks, in Ringer's solution. Total test duration: 1800 s ($n = 3$).

This work also analyzed the evolution of the frictional coefficient. The results obtained are presented in Figure 5. For Samples 1 and 5, the frictional coefficient showed a decrease around 900 and 600 s, respectively, stabilizing for the remainder of the experiment. Samples 2 and 4 showed stable behavior during the test, and Sample 3 showed a uniform evolution. These coefficients are in the order of 10% of the frictional force, which is consistent with the fact that the normal force is of the order of 10 N. An alternative perspective, albeit infrequently employed, involves examining the variation in normal force as a function of changes in the coefficient of friction, as illustrated in Figure 6. The wear rate, defined as the wear volume *per* track distance, was calculated for each type of surface finishing. The results are presented in Figure 7.

The tribological tests start with normal forces at 10 N, then for Samples 1, 2, and 4, this value rapidly decreases to normal forces between 8 and 9 N. Analogously to what is

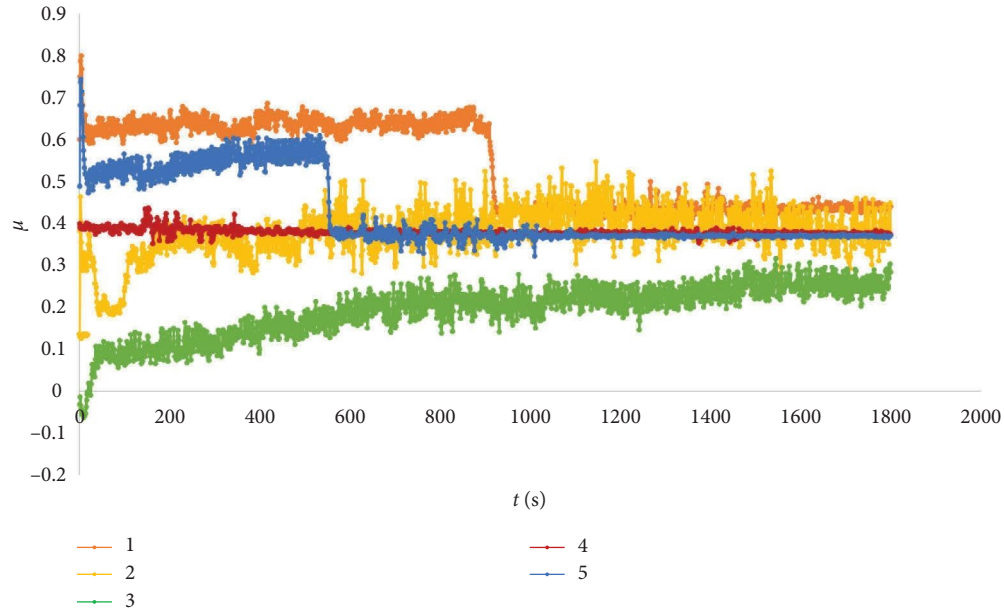

FIGURE 5: Frictional coefficient variation in function of time for all types of tribology disks, in Ringer's solution. Total test duration: 1800 s ($n = 3$).

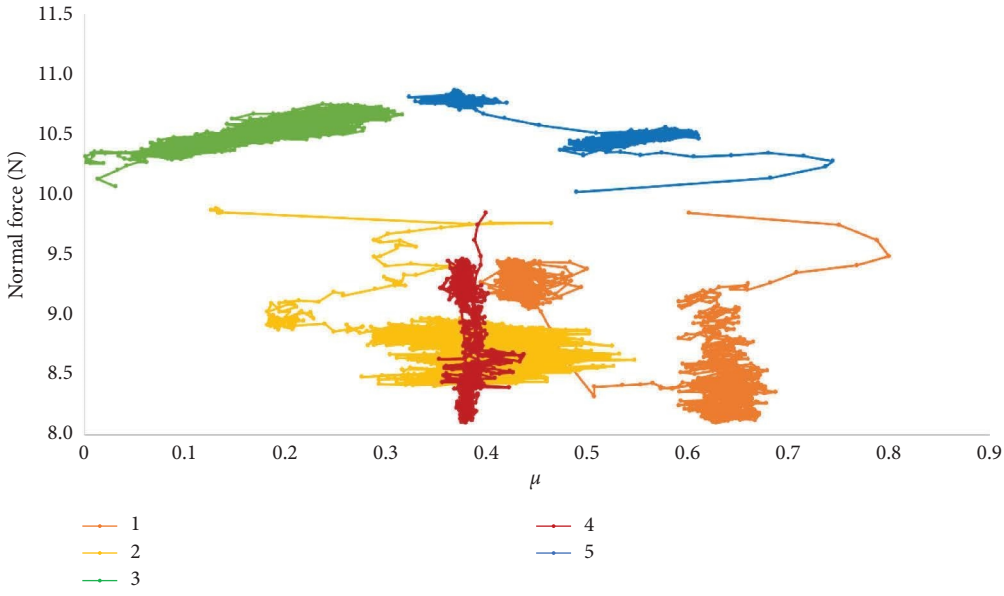

FIGURE 6: The relationship between normal force and coefficient of friction ($n = 3$).

seen in Figure 5, Sample 4 presented a homogeneous coefficient behavior.

Figure 7 depicts the wear rate of five different titanium alloy samples following ball cratering wear tests. It can be observed that Samples 2, 3, and 4 exhibit lower wear rates, while Sample 5 demonstrates higher values. This reduction in the wear rate could be attributed to an increase in the hardness of the samples. Consistent findings have been reported with similar tests conducted on different tribological systems [40].

The tribological evaluation associated with the corrosion chronoamperometry, for all five disks, is shown in Figures 8, 9, and 10. The frictional coefficient as a function of time presented a homogeneous behavior for all samples evaluated.

Similar to the information provided above, Figure 9 illustrates the evolution of the frictional coefficient results. These coefficients are in the order of 10% of the frictional force, which is consistent with the fact that the normal force is of the order of 10 N [40–44].

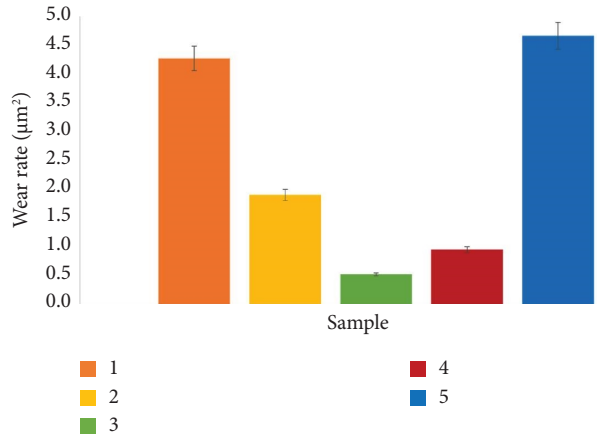

FIGURE 7: Wear rate (μm^2) for each type of tribology disk, after corrosion potential monitoring. Data were assessed using two-way ANOVA followed by Tukey's test ($n = 3$). ($p < 0.05$).

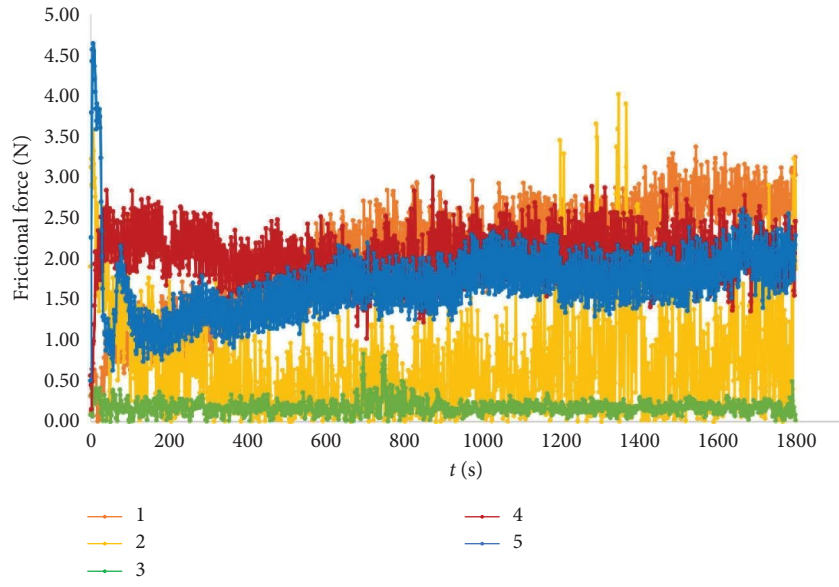

FIGURE 8: Frictional force variation in function of time for all types of tribology disks, in Ringer's solution, monitored during chronoamperometry tests. Total test duration: 1800 s ($n = 3$).

According to the criterion proposed by Stack and Abdulrahman [45], which has been used for Ti-6Al-4V, the degradation mechanism under the anodic potentials at every normal force stage is classified as 'wear-corrosion,' and it could be implied that the wear track on Ti-6Al-4V discs is enlarged by the action of the third body wear particles.

The wear rate for the five different titanium alloy samples after the ball cratering wear tests is shown in Figure 10. It is possible to observe that the wear rate is inferior for Samples 2, 3, and 4, being the highest values associated with Sample 5. This tendency is in accordance with the wear rate shown previously in Figure 7.

The changes in the mean current can be related to the enlargement of the contacting area with the number of tribocorrosion cycles. According to Mischler et al. [46], the mean abrasion of the oxide thin film decreases with the tribocorrosion cycles.

3.2. Tribological Analyses. The EBM Ti-6Al-4V–ELI samples were also characterized by conventional tribological tests, not concomitant with corrosion evaluation. Two types of analyses were done: with Ringer's solution and without this (in air). It is known that this saline solution acts as a lubricant for tribology. The results for the frictional coefficient and wear rate are shown in Figures 11, 12, 13, and 14. The frictional force results are not shown; as presented earlier, it has a relation directly proportional to the frictional coefficient values, that is, 10 times greater.

In Figure 11, for Samples 1 and 5, the frictional coefficient showed a decrease of 900 and 600 s, respectively, remaining stable after this for the remainder of the experiment time. Samples 2 and 4 showed stable behavior during the test, and in Sample 3, the coefficient started at inferior values, rapidly increased, and showed a uniform evolution, reaching the highest value, compared to the

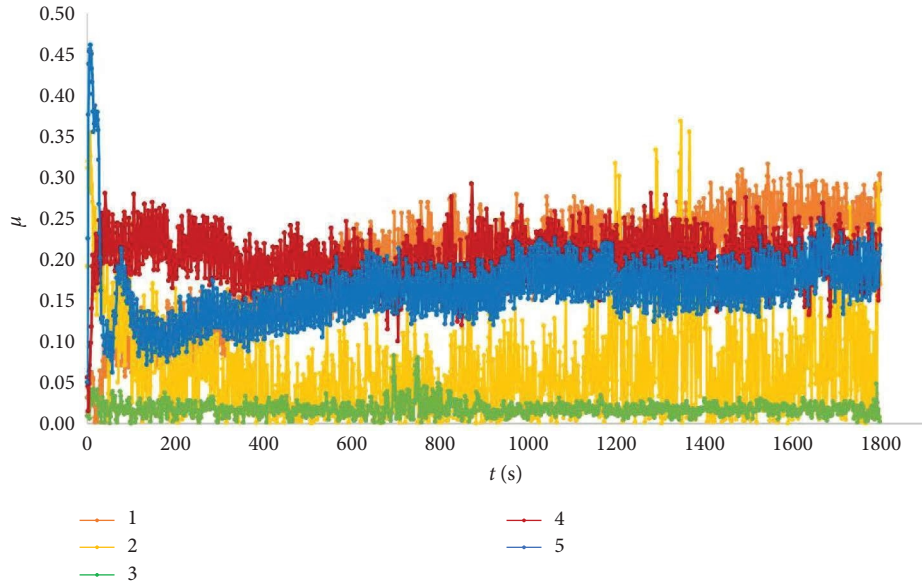

FIGURE 9: Frictional coefficient variation in function of time for all types of tribology disks, in Ringer's solution, monitored during chronoamperometry tests. Total test duration: 1800 s ($n = 3$).

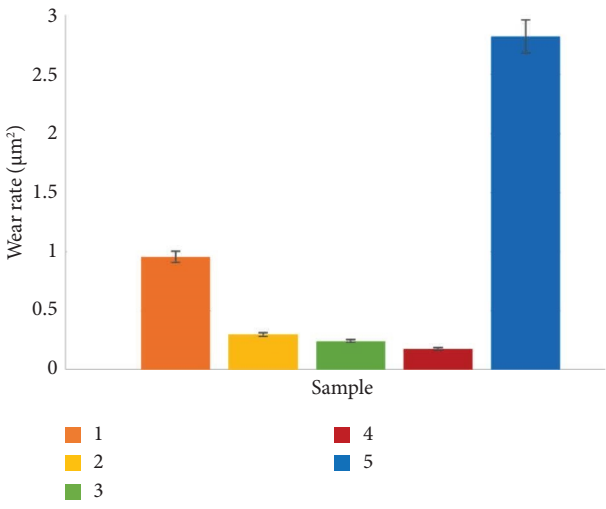

FIGURE 10: Wear rate (μm^2) for each type of tribology disk, after chronoamperometry tests. Data were assessed using two-way ANOVA followed by Tukey's test ($n = 3$) ($p < 0.05$).

other samples. The frictional coefficient for the tribological analyses with lubrication presented a similar behavior to that obtained in the tribocorrosion tests, monitoring the OCP, that is, without applying any overvoltage. These tribological tests were repeated three times to ensure the reproducibility of the results.

Figure 12 presents the wear rate for the five different titanium alloy samples after the ball cratering wear tests. It is possible to observe that the wear rate is inferior for Samples 2, 3, and 4, being the highest values associated with Sample 5. This tendency is in accordance with the wear rate shown previously in Figures 7 and 10.

In Figure 13, the frictional coefficient showed stable behavior during all tests, for Samples 1, 2, and 5, with values around 0.8 and 1.0. Sample 3 showed a stable behavior during the test, with values around 0.3, and Sample 4 showed an increase up to 500 s, and then a stable evolution to the end of the evaluation.

Figure 14 presents the wear rate for the five different titanium alloy samples after the ball cratering wear tests. It is possible to observe that the wear rate is inferior for Samples 2, 3, and 4, being the higher values associated with Sample 1. This tendency is in accordance with the wear rate shown in the previous figures. Comparing the wear rate results shown in Figures 7, 10, 12, and 14, the wear rate is associated with the effect of electrolyte (Ringer's solution) that plays a dual role; in some cases, it acts as a corrosive environment, while in others, it acts as a tribology lubricant. Figure 15 illustrates a macrography depicting the wear tracks generated on the surfaces of the tribology disks. Confocal microscopy was used to verify the tribological path generated on the surfaces, as well as the electrochemical attack. These results are presented in Figures 16(a), 16(b), 16(c), 16(d), and 16(e).

The macrography (Figure 15) and the confocal microscopy images (Figure 16) qualitatively present the sample's roughness. It is known that surface finishings play a significant role in various surface phenomena such as electrochemical and tribological performance.

Fouzia et al. [47] studied some morphological and mechanical properties of nanostructured Ti-6Al-4Fe alloys manufactured by powder metallurgy with varying ball milling times, compacted, and followed by sintering. They found an increase in density of the alloys due to the reduction in porosity with increasing milling time of the powder. Additionally, the surface roughness decreased with milling time of the powders for the developed Ti-6Al-4Fe alloys.

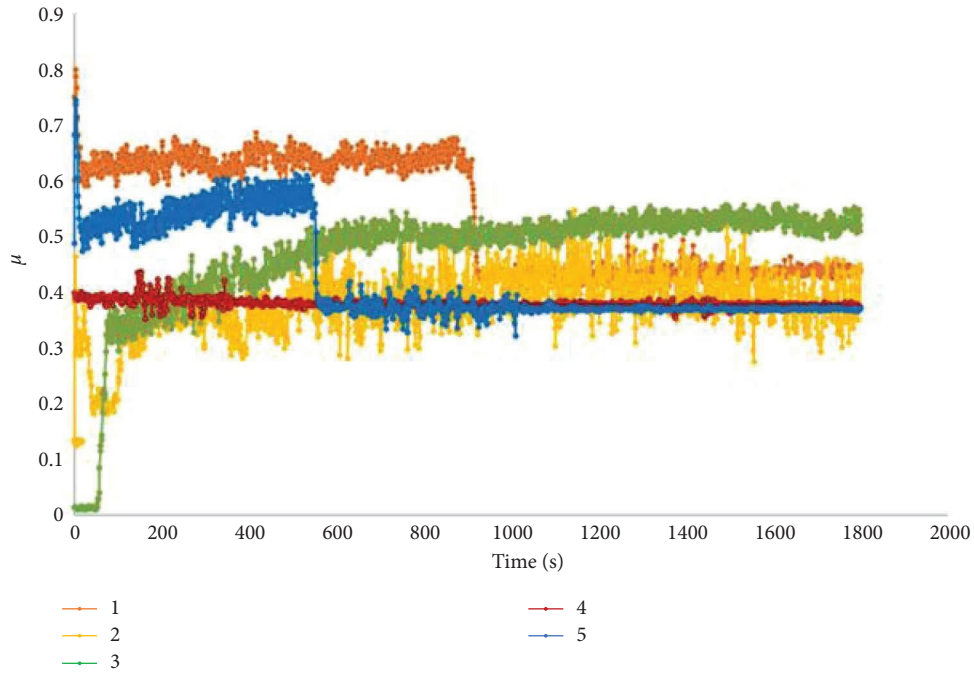

FIGURE 11: Frictional coefficient variation in function of time for all types of tribology disks, in Ringer's solution, without corrosion tests. Total test duration: 1800 s ($n = 3$).

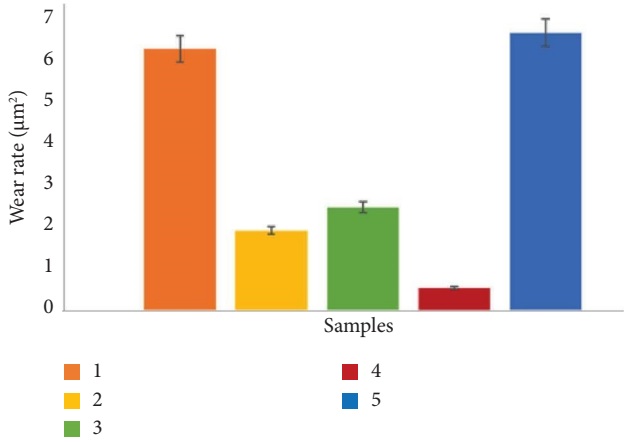

FIGURE 12: Wear rate (μm^2) for each type of tribology disk, in Ringer's solution, without corrosion tests. Data were assessed using two-way ANOVA followed by Tukey's test. ($n = 3$) ($p < 0.05$).

Surface finishings are an important parameter for biomaterials as they influence functionality and biocompatibility with human tissues. The transition zone shown in Figure 16 illustrates the tribocorrosion effect on these biomaterial samples.

The roughness parameters presented in Table 2 are as follows: Ra (arithmetic mean of the absolute departures of the roughness profile from the mean line), both before and after the tribocorrosion tests. All the obtained values are in accordance with those reported in the literature for titanium alloys used for biomedical applications [48]. As detailed in the methodology, since all samples had identical surface finishes, no significant differences in roughness were anticipated prior to the tribocorrosion tests. At the end of the trials, the highest Ra values were obtained for Samples 5 and 1, respectively.

Wear occurs at the interface of contacting materials and is significantly impacted by the surface finish from the EBM process.

Feyzi et al. [38] evaluated the tribocorrosion behavior of Ti-6Al-4V alloy under its normal force and electrochemical potential. They have found neither a direct nor reverse relationship with the normal force. One tribocorrosion cycle begins with depassivation and finishes with repassivation. On the mechanical aspect, the coefficient of friction increases with decreasing normal force.

The roughness of the disks before and after the tribocorrosion tests was evaluated using confocal microscopy, which showed no significant differences in roughness before testing. Hammood et al. [49] examined how different surface roughness affects the tribocorrosion behavior of Ti-6Al-4V. Their study found that increasing contact load results in a lower average tribocorrosion current density on smoother surfaces compared to rougher ones, indicating that damage is more apparent on the smooth surface.

The confocal microscopy also shows dark regions, associated with the oxidation of the basis metallic biomaterial and sharp regions related to the wear tracks. Even during electrochemical tests, mechanical wear removes its surface layer and prevents oxidation of the surfaces due to exposure to corrosive attack in Ringer's saline solution medium.

Confocal microscopy and electrochemical current measurements demonstrated that chemical losses significantly contributed to the total material loss in the anodic

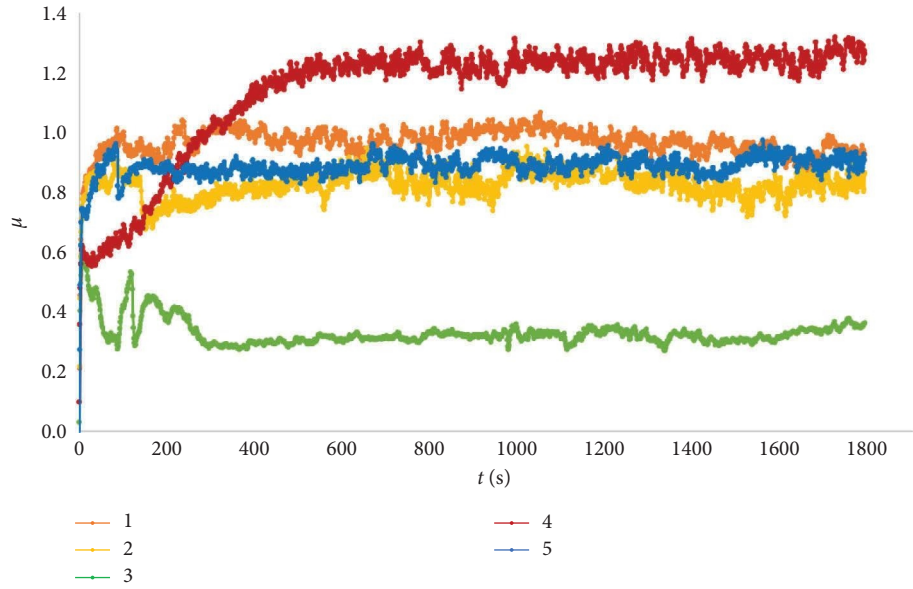

FIGURE 13: Frictional coefficient variation in function of time for all types of tribology disks, without lubrication. Total test duration: 1800 s ($n = 3$).

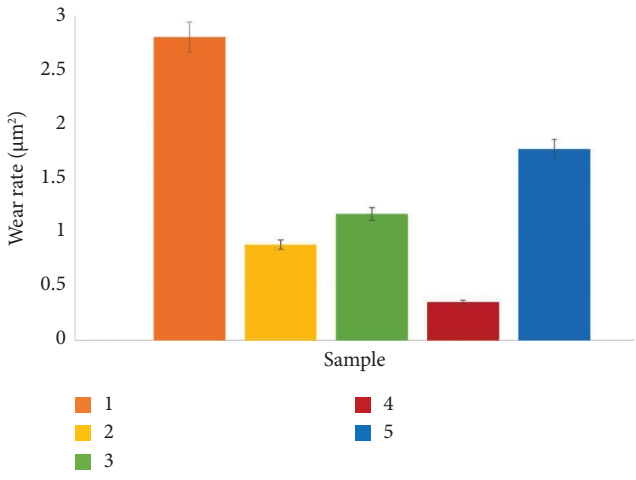

FIGURE 14: Wear rate (μm^2) for each type of tribology disk, without lubrication. Data were assessed using two-way ANOVA followed by Tukey's test. ($n = 3$) ($p < 0.05$).

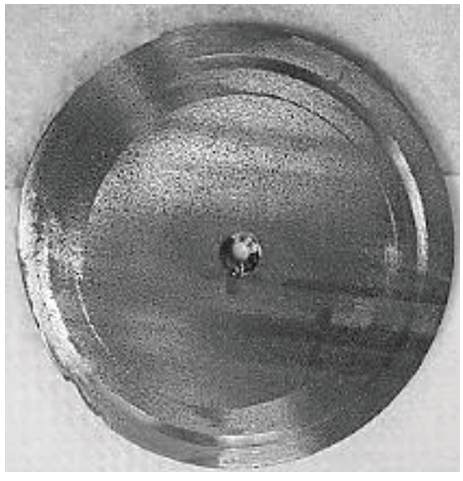

FIGURE 15: Macrography of a tribology EBM Ti-6Al-4V-ELI disk after several tribocorrosion tests (without magnification). ($n = 3$).

region. In this domain, material loss increased with the potential level due to the formation of an oxide layer, which may result in enhanced shear cutting. Conversely, in the cathodic domain, hydrogen embrittlement altered the properties of the interface, thus affecting the extent of material loss. Both the mechanical and chemical wear were described by an existing tribocorrosion theory [38].

Frictional coefficient evaluation attained different values according to the tribology assessment done. In tribocorrosion tests, analyzing the corrosion OCP, the coefficient of friction presented values around 0.1 and 0.65, but concerning tribocorrosion tests analyzing the current densities, the coefficient of friction presented values around 0 and 0.45. For the tribological tests with lubrication, the frictional coefficient showed values of about 0.2 and 0.6, and without lubrication, values of around 0.3 and 1.3. The lowest values were obtained for the chronoamperometry tests, due to the samples' polarization at 0.4 ($V/_{Ag/AgCl}$) in association with the tribological effect. Conversely, the highest tribological values were observed without corrosion or lubrication, as lubrication reduces wear and friction according to the literature [50–52].

The effect of the variation of the coefficient of friction as a function of the test time was studied by Huang et al. [50]. They verified tribological properties in Ti-6Al-4V alloys, both with and without coating ("laser clad"), throughout 3500 s in different rotation frequencies, and at the end of the tests, verified that the coefficient of friction for the coatings was always inferior to the substrate.

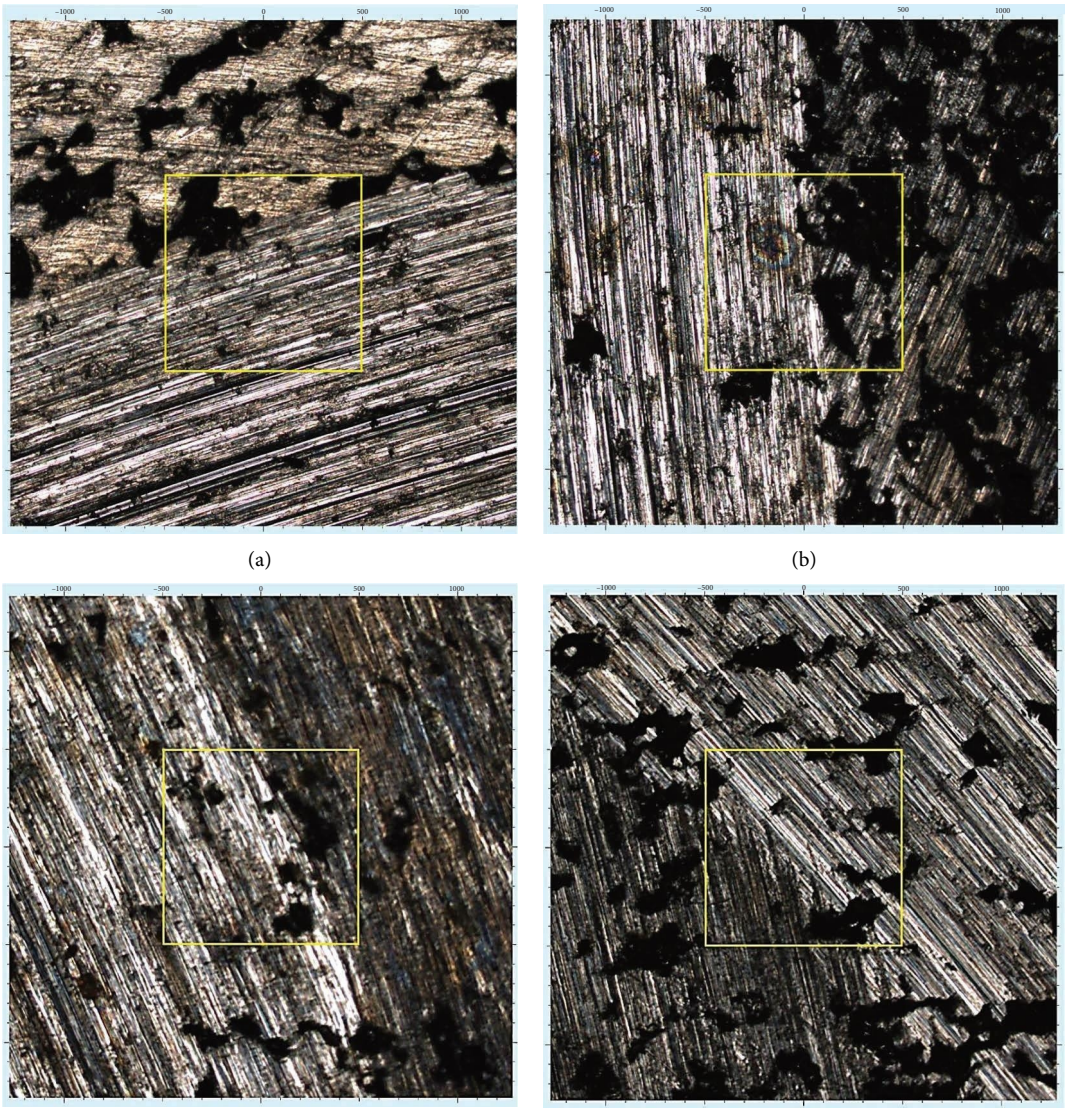

(a) (b) (c) (d)

Figure 16: Continued.

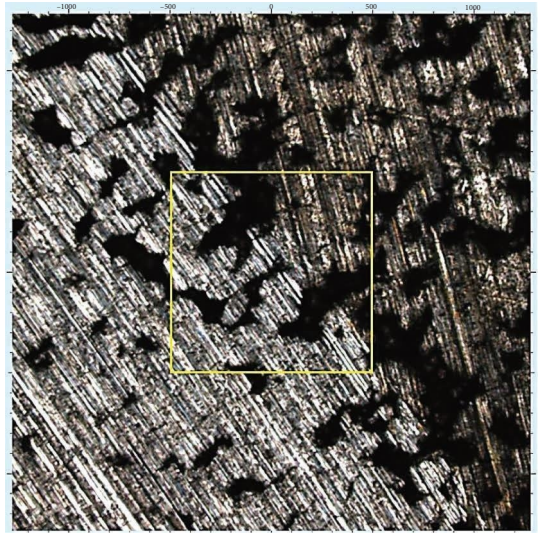

(e)

Figure 16: (a) Confocal microscopy image for Sample 1, after tribocorrosion evaluation test. The square emphasis on the transition zone, above: the disk, and below: the wear track ($n = 6$). (b) Confocal microscopy image for Sample 2, after tribocorrosion evaluation test. The square emphasizes the transition zone. On the right: the disk, and on the left: the wear track and oxidation spots ($n = 6$). (c) Confocal microscopy image for Sample 3, after the tribocorrosion evaluation test. The square emphasizes the transition zone. On the right: the disk, and on the left: the wear path ($n = 6$). (d) Confocal microscopy image for Sample 4, after tribocorrosion evaluation test. The square emphasizes the transition zone. In the bottom left: the disk, and in the top right: the wear track ($n = 6$). (e) Confocal microscopy image for Sample 5, after tribocorrosion evaluation test. The square emphasizes the transition zone. On the right: the disk, and on the left: the wear track ($n = 6$).

Table 2: Roughness parameters of EBM Ti-6Al-4V-ELI disks measured by CLSM, both before and after the tribocorrosion tests ($n = 6$).

Surface	Ra (μm) (before)	Ra (μm) (after)
1	0.340 ± 0.177	0.625 ± 0.212
2	0.300 ± 0.211	0.440 ± 0.213
3	0.326 ± 0.103	0.458 ± 0.308
4	0.319 ± 0.221	0.411 ± 0.188
5	0.385 ± 0.186	0.787 ± 0.123

The tribocorrosion behavior of Ti-6Al-4V-ELI, especially its oxide film dynamics, involves a combined effect of mechanical wear and corrosion. The Ti-6Al-4V alloy naturally develops a thin, protective oxide layer in physiological environments, which acts as a barrier to prevent direct contact between the metal and the corrosive bodily fluids. However, mechanical interactions can damage this layer, speeding up corrosion. Understanding how the oxide film breaks down and reforms, along with the impact of factors such as applied load, sliding frequency, and the environment, is essential for enhancing the long-term performance of Ti-6Al-4V-ELI implants [50–52].

Concomitant tests in tribology and electrochemistry make it possible to monitor the passive film, that is, to verify its breakdown and its recovery or regrowth [51, 52].

4. Conclusions

AM techniques have revolutionized the design and processing of implantable medical and dental devices for hard tissue regeneration. In this paper, the influence of five different scanning speeds on the tribocorrosion behavior of the electron beam–melted Ti-6Al-4V-ELI was investigated.

The tribological behavior is influenced by the type of finishing surface produced with EBM Ti-6Al-4V-ELI in different scanning speed processes used for this biomaterial.

Friction coefficient and frictional force are dependent on the normal force and the sample's roughness. The wear rate values are dependent on the EBM parameters' variation. The surface characterization by confocal microscopy showed the transition zone, that is, the basis metallic material and the removed area on the wear tracks.

Tribocorrosion is not just wear or corrosion; it is the synergistic effect of both. The mechanical wear accelerates corrosion, and corrosion can weaken the material, making it more susceptible to wear.

The combined effect of mechanical wear and electrochemical damage was evident in the tribocorrosion tests. Potentiometry and chronoamperometry analyses showed the passive film behavior, naturally formed on this biomaterial's surface, as a function of immersion time. Following the tribological tests, the OCP returned to more noble values, with the lowest potentials observed for Disks 1 and 3. The mean wear rate of the passive layer decreased with the tribocorrosion cycles.

Findings from this research may assist future optimization by guiding the selection of suitable EBM parameters for specific clinical needs, such as maximizing strength, ductility, wear, or corrosion resistance, and decreasing surface roughness or porosity. By applying these findings,

EBM can be further improved to produce high-quality, biocompatible, and cost-effective implants tailored to specific clinical applications. This includes enhancing material properties, geometric accuracy, and process efficiency.

Data Availability Statement

The raw/processed data required to reproduce these findings cannot be shared at this time, as the data also contain part of an ongoing study.

Ethics Statement

The authors hereby approve that the principles of ethical and professional conduct have been followed in the work. The present research does not involve any human or animal participation.

Consent

The authors and the authorities at the institute/organization where this work has been carried out give their explicit consent to submit and publish the work, if found suitable.

Conflicts of Interest

The authors declare no conflicts of interest.

Funding

This work was supported by Conselho Nacional de Desenvolvimento Científico e Tecnológico - CNPq – (Process: 443931/2023-2) and by Instituto de Pesquisas Energéticas e Nucleares – IPEN/CNEN - (Project 07, Edital 06/2020).

Acknowledgments

This work was supported by Conselho Nacional de Desenvolvimento Científico e Tecnológico - CNPq (Process: 443931/2023-2) and by Instituto de Pesquisas Energéticas e Nucleares—IPEN/CNEN (Project 07, Edital 06/2020).

References

[1] E. F. Pieretti, E. J. Pessine, O. V. Correa, W. de Rossi, and M. D. M. das Neves, "Effect of Laser Parameters on the Corrosion Resistance of the ASTM F139 Stainless Steel," *International Journal of Electrochemical Science* 10, no. 2 (2015): 1221–1232, https://doi.org/10.1016/s1452-3981(23)05067-8.

[2] E. F. Pieretti, T. P. Leivas, M. F. Pillis, and M. D. M. Das Neves, "Failure Analysis of Metallic Orthopedic Implant for Total Knee Replacement," *Materials Science Forum* 1012 (2020): 471–476, https://doi.org/10.4028/www.scientific.net/msf.1012.471.

[3] E. F. Pieretti and I. Costa, "Surface Characterisation of ASTM F139 Stainless Steel Marked by Laser and Mechanical Techniques," *Electrochimica Acta* 114 (2013): 838–843, https://doi.org/10.1016/j.electacta.2013.05.101.

[4] E. F. Pieretti, S. M. Manhabosco, L. F. P. Dick, S. Hinder, and I. Costa, "Localized Corrosion Evaluation of the ASTM F139 Stainless Steel Marked by Laser Using Scanning Vibrating Electrode Technique, X-Ray Photoelectron Spectroscopy and Mott-Schottky Techniques," *Electrochimica Acta* 124 (2014): 150–155, https://doi.org/10.1016/j.electacta.2013.10.137.

[5] R. A. Marques, S. O. Rogero, M. Terada, E. F. Pieretti, and I. Costa, "Localized Corrosion Resistance and Cytotoxicity Evaluation of Ferritic Stainless Steels for Use in Implantable Dental Devices With Magnetic Connections," *International Journal of Electrochemical Science* 9, no. 3 (2014): 1340–1354, https://doi.org/10.1016/s1452-3981(23)07798-2.

[6] S. M. Manhabosco, Á. Pritzel dos Santos, M. L. Marcolin, E. F. Pieretti, M. D. M. Neves, and L. F. P. Dick, "Localized Corrosion of Laser Marked M340 Martensitic Stainless Steel for Biomedical Applications Studied by the Scanning Vibrating Electrode Technique Under Polarization," *Electrochimica Acta* 200 (2016): 189–196, https://doi.org/10.1016/j.electacta.2016.03.178.

[7] E. F. Pieretti, R. P. Palatnic, T. P. Leivas, I. Costa, and M. D. M. das Neves, "Phosphate Buffer Solution With Albumin," *International Journal of Electrochemical Science* 9, no. 5 (2014): 2435–2444, https://doi.org/10.1016/s1452-3981(23)07938-5.

[8] E. F. Pieretti, I. Costa, R. A. Marques, T. P. Leivas, and M. D. M. das Neves, "Electrochemical Study of a Laser Marked Biomaterial in Albumin Solution," *International Journal of Electrochemical Science* 9, no. 7 (2014): 3828–3836, https://doi.org/10.1016/s1452-3981(23)08054-9.

[9] M. Fousová, D. Vojtech, K. Doubrava, M. Matej Daniel, and C.-F. Lin, "Influence of Inherent Surface and Internal Defects on Mechanical Properties of Additively Manufactured Ti6Al4V Alloy: Comparison Between SLM and EBM. Metal Industries Research & Development Centre," *Materials* 11, no. 537 (2018): 1–18, https://doi.org/10.3390/ma11040537.

[10] C. Yan, L. Hao, A. Hussein, and P. Young, "Ti–6Al–4V Triply Periodic Minimal Surface Structures for Bone Implants Fabricated via Selective Laser Melting," *Journal of the Mechanical Behavior of Biomedical Materials* 51 (2015): 61–73, https://doi.org/10.1016/j.jmbbm.2015.06.024.

[11] Q. Wang, P. Zhou, S. Liu, et al., "Multi-Scale Surface Treatments of Titanium Implants for Rapid Osseointegration: A Review-Metal Industries Research & Development Centre," *Nanomaterials* 10, no. 1244 (2020): 1–27.

[12] P. Pou, A. Riveiro, J. Val, et al., "Laser Surface Texturing of Titanium for Bioengineering Applications," *Procedia Manufacturing* 13 (2017): 694–701.

[13] S. J. Ferguson, N. Broggini, M. Wieland, et al., "Biomechanical Evaluation of the Interfacial Strength of a Chemically Modified Sandblasted and Acid-Etched Titanium Surface," *Journal of Biomedical Materials Research Part A* (2006): 291–297, https://doi.org/10.1002/jbm.a.30678.

[14] I. Drstvensek, N. I. Hren, T. Strojnik, T. Brajlih, and B. Valentan, "Applications of Rapid Prototyping in Cranio-Maxilofacial Surgery Procedures," *Internal Journal of Biology and Biomedical Engineering* 2, no. 1 (2008): 29–38.

[15] A. Ataee, Y. Li, and C. Wen, "A Comparative Study on the Nanoindentation Behavior, Wear Resistance and In Vitro Biocompatibility of SLM Manufactured CP-Ti and EBM Manufactured Ti64 Gyroid Scaffolds," *Acta Biomaterialia* 97 (2019): 587–596, https://doi.org/10.1016/j.actbio.2019.08.008.

[16] A. Wennerberg and T. Albrektsson, "Effects of Titanium Surface Topography on Bone Integration: A Systematic Review," *Clinical Oral Implants Research* 20, no. s4 (2009): 172–184, https://doi.org/10.1111/j.1600-0501.2009.01775.x.

[17] E. F. Pieretti, O. V. Corrêa, M. D. M. Neves, R. A. Antunes, and M. F. Pillis, "Tribology Analysis on Anodized Aluminum

Surfaces for Biomedical Purposes," *Brazilian Journal of Motor Behavior* 17 (2023): 196–197.

[18] F. Trevisan, F. Calignano, A. Aversa, et al., "Additive Manufacturing of Titanium Alloys in the Biomedical Field: Processes, Properties and Applications," *Journal of Applied Biomaterials & Functional Materials* 16, no. 2 (2018): 57–67, https://doi.org/10.5301/jabfm.5000371.

[19] A. T. Silvestri, S. Foglia, R. Borrelli, S. Franchitti, C. Pirozzi, and A. Astarita, "Electron Beam Melting of Ti6Al4V: Role of the Process Parameters Under the Same Energy Density," *Journal of Manufacturing Processes* 60 (2020): 162–179, https://doi.org/10.1016/j.jmapro.2020.10.065.

[20] L. Zhang, Y. Liu, S. Li, and Y. Hao, "Additive Manufacturing of Titanium Alloys by Electron Beam Melting: A Review," *Advanced Engineering Materials* 20, no. 5 (2017): 1700842, https://doi.org/10.1002/adem.201700842.

[21] S. I. G. Fangaia, A. Messias, F. A. D. R. A. Guerra, A. C. F. Ribeiro, A. J. M. Valente, and P. M. G. Nicolau, "Evaluation of the Tribocorrosion Behavior of Ti-6Al-4V Biomedical Alloy in Simulated Oral Environments," *Processes* 12, no. 7 (2024): 1283, https://doi.org/10.3390/pr12071283.

[22] S. Lavrys, I. Pohrelyuk, H. Veselivska, A. Skrebtsov, J. Kononenko, and Y. Marchenko, "Corrosion Behavior of Near-Alpha Titanium Alloy Fabricated by Additive Manufacturing," *Materials and Corrosion* 73, no. 12 (2022): 2063–2070, https://doi.org/10.1002/maco.202213105.

[23] J. Quinn, R. McFadden, C. W. Chan, and L. Carson, "Titanium for Orthopedic Applications: An Overview of Surface Modification to Improve Biocompatibility and Prevent Bacterial Biofilm Formation," *iScience* 23, no. 11 (2020): 101745–22, https://doi.org/10.1016/j.isci.2020.101745.

[24] D. H. Abdeen and B. R. Palmer, "Corrosion Evaluation of Ti-6Al-4V Parts Produced With Electron Beam Melting Machine," *Rapid Prototyping Journal* 22, no. 2 (2016): 322–329, https://doi.org/10.1108/rpj-09-2014-0104.

[25] V. Dehnavi, J. D. Henderson, C. Dharmendra, et al., "Corrosion Behaviour of Electron Beam Melted Ti6Al4V: Effects of Microstructural Variation," *Journal of the Electrochemical Society* 167, no. 13 (2020): 131505, https://doi.org/10.1149/1945-7111/abb9d1.

[26] X. He, J. J. Noël, and D. W. Shoesmith, "Temperature Effects on Oxide Film Properties of Grade-7 Titanium," *Corrosion* 63, no. 8 (2007): 781–792, https://doi.org/10.5006/1.3278427.

[27] T. Sugahara, D. A. P. Reis, C. Moura Neto, et al., "The Effect of Widmanstätten and Equiaxed Microstructures of Ti–6Al–4V on the Oxidation Rate and Creep Behavior," *Materials Science Forum* 636-637 (2010): 657.

[28] P. Herrera, E. Hernandez-Nava, R. Thornton, and T. Slatter, "Abrasive Wear Resistance of Ti-6AL-4V Obtained by the Conventional Manufacturing Process and by Electron Beam Melting (EBM)," *Wear* 524-525 (2023): 204879–204910, https://doi.org/10.1016/j.wear.2023.204879.

[29] D. Sharma, M. Kamran, N. K. Paraye, and R. Anant, "Insights Into the Wear Behaviour of Electron Beam Melted Ti–6Al–4V Alloy in the As-Built and the Heat-Treated Conditions," *Journal of Manufacturing Processes* 71 (2021): 669–678, https://doi.org/10.1016/j.jmapro.2021.09.060.

[30] T. N. Q. Costa, T. C. Dotta, R. Galo, M. E. d.C. Soares, and V. Pedrazzi, "Effect of Tribocorrosion on Surface-Treated Titanium Alloy Implants: A Systematic Review With Meta-Analysis," *Journal of the Mechanical Behavior of Biomedical Materials* 145 (2023): 106008, https://doi.org/10.1016/j.jmbbm.2023.106008.

[31] D. F. Ferreira, S. M. A. Almeida, R. B. Soares, et al., "Synergism Between Mechanical Wear and Corrosion on Tribocorrosion of a Titanium Alloy in a Ringer Solution," *Journal of Materials Research and Technology* 8, no. 2 (2019): 1593–1600, https://doi.org/10.1016/j.jmrt.2018.11.004.

[32] I. Hacisalihoglua, A. Samancioglub, F. Yildiza, G. Purcekc, and A. Alsaran, "Tribocorrosion Properties of Different Type Titanium Alloys in Simulated Body Fluid," *Wear* (2015): 1–8.

[33] J. Shittu, M. Pole, S. Muskeri, et al., "Tribo-Corrosion Response of Additively Manufactured High-Entropy Alloy," *Materials Degradation* 5, no. 31 (2021): 1–8.

[34] M. Buciumeanu, A. Bagheri, N. Shamsaei, S. M. Thompson, F. S. Silva, and B. Henriques, "Tribocorrosion Behavior of Additive Manufactured Ti-6Al-4V Biomedical Alloy," *Tribology International* 119 (2018): 381–388, https://doi.org/10.1016/j.triboint.2017.11.032.

[35] F. Toptan, A. C. Alves, O. Carvalho, et al., "Corrosion and Tribocorrosion Behaviour of Ti6Al4V Produced by Selective Laser Melting and Hot Pressing in Comparison With the Commercial Alloy," *Journal of Materials Processing Technology* 266 (2019): 239–245, https://doi.org/10.1016/j.jmatprotec.2018.11.008.

[36] J. Huang, Y. Huang, X. Yu, G. Liu, S. Yu, and D. Fan, "Corrosion Characterization of Ti-6Al-4V Coating Layer by the Alternating Current Assisted GTAW Method," *Corrosion Science* 197 (2022): 110066, https://doi.org/10.1016/j.corsci.2021.110066.

[37] M. Fellah, N. Bouchareb, N. Hezil, et al., "Electrochemical Analysis of Mechanically Alloyed Ti50%-Ni50% Alloy for Bone Implants Use," *Journal of Alloys and Compounds* 1010 (2025): 178046, https://doi.org/10.1016/j.jallcom.2024.178046.

[38] M. Feyzi, K. Fallahnezhad, M. Taylor, and R. Hashemi, "The Tribocorrosion Behaviour of Ti-6Al-4 V Alloy: The Role of Both Normal Force and Electrochemical Potential," *Tribology Letters* 70, no. 3 (2022): 83, https://doi.org/10.1007/s11249-022-01624-0.

[39] L. Odehnal, M. Ranuša, M. Vrbka, I. Křupka, and M. Hartl, "Tribological Behaviour of Ti6Al4V Alloy: An Application in Small Joint Implants," *Tribology Letters* 71, no. 4 (2023): 125, https://doi.org/10.1007/s11249-023-01795-4.

[40] R. C. Cozza, D. K. Tanaka, and R. M. Souza, "Friction Coefficient and Abrasive Wear Modes in Ball-Cratering Tests Conducted at Constant Normal Force and Constant Pressure–Preliminary Results," *Wear* 267, no. 1-4 (2009): 61–70, https://doi.org/10.1016/j.wear.2009.01.055.

[41] R. C. Cozza, J. D. B. de Mello, D. K. Tanaka, and R. M. Souza, "Relationship Between Test Severity and Wear Mode Transition in Micro-Abrasive Wear Tests," *Wear* 263, no. 1-6 (2007): 111–116, https://doi.org/10.1016/j.wear.2007.01.099.

[42] R. C. Cozza, "Influence of the Normal Force, Abrasive Slurry Concentration and Abrasive Wear Modes on the Coefficient of Friction in Ball-Cratering Wear Tests," *Tribology International* 70 (2014): 52–62, https://doi.org/10.1016/j.triboint.2013.09.010.

[43] R. I. Trezona, D. N. Allsopp, and I. M. Hutchings, "Transitions Between Two-Body and Three-Body Abrasive Wear: Influence of Test Conditions in the Microscale Abrasive Wear Test," *Wear* 225-229 (1999): 205–214, https://doi.org/10.1016/s0043-1648(98)00358-5.

[44] R. C. Cozza, D. K. Tanaka, and R. M. Souza, "Friction Coefficient and Wear Mode Transition in Micro-Scale Abrasion Tests," *Tribology International* 44, no. 12 (2011): 1878–1889, https://doi.org/10.1016/j.triboint.2011.08.006.

[45] M. Stack and G. Abdulrahman, "Mapping Erosion-Corrosion of Carbon Steel in Oil Exploration," *Tribology International* (2010).

[46] S. Mischler, S. Debaud, and D. Landolt, "Wear-Accelerated Corrosion of Passive Metals in Tribocorrosion Systems," *Journal of the Electrochemical Society* 145, no. 3 (1998): 750–758, https://doi.org/10.1149/1.1838341.

[47] H. Fouzia, F. Mamoun, H. Naouel, et al., "The Effect of Milling Time on the Microstructure and Mechanical Properties of Ti-6Al-4Fe Alloys," *Materials Today Communications* 27 (2021): 102428, https://doi.org/10.1016/j.mtcomm.2021.102428.

[48] S. Ponader, E. Vairaktaris, P. Heinl, et al., "Effects of Topographical Surface Modifications of Electron Beam Melted Ti-6Al-4V Titanium on Human Fetal Osteoblasts," *Journal of Biomedical Materials Research Part A* 84, no. 4 (2007): 1111–1119, https://doi.org/10.1002/jbm.a.31540.

[49] A. S. Hammood, L. Thair, H. D. Altawaly, and N. Parvin, "Tribocorrosion Behaviour of Ti–6Al–4V Alloy in Biomedical Implants: Effects of Applied Load and Surface Roughness on Material Degradation," *Journal of Bio- and Tribo-Corrosion* 5, no. 4 (2019): 85–98, https://doi.org/10.1007/s40735-019-0277-x.

[50] C. Huang, Y. Zhang, R. Vilar, and J. Shen, "Dry Sliding Wear Behavior of Laser Clad TiVCrAlSi High Entropy Alloy Coatings on Ti-6Al-4V Substrate," *Materials & Design* 41 (2012): 338–343, https://doi.org/10.1016/j.matdes.2012.04.049.

[51] F. Liu, J. Fisher, and Z. Jin, "Effect of Motion Inputs on the Wear Prediction of Artificial Hip Joints," *Tribology International* 63 (2013): 105–114, https://doi.org/10.1016/j.triboint.2012.05.029.

[52] N. Diomidis, S. Mischler, N. S. More, and M. Roy, "Tribo-Electrochemical Characterization of Metallic Biomaterials for Total Joint Replacement," *Acta Biomaterialia* 8, no. 2 (2012): 852–859, https://doi.org/10.1016/j.actbio.2011.09.034.